NOTES AND CORRESPONDENCE

An Examination of the AGCM Simulated Surface Wind Stress and Low-Level Winds over the Tropical Pacific Ocean

BOHUA HUANG AND J. SHUKLA

Center for Ocean–Land–Atmosphere Studies, Calverton, Maryland

22 May 1995 and 25 July 1995

ABSTRACT

The monthly mean surface wind stress and winds in the lower troposphere for 1986–92 simulated by the Center for Ocean–Land–Atmosphere Studies atmospheric general circulation model (AGCM) forced with observed sea surface temperature (SST) is compared with observations. It is found that the AGCM surface stress has weak equatorial easterlies during boreal spring and weak El Nin ˜o–Southern Oscillation (ENSO) signals over the central and eastern Pacific Ocean. On the other hand, the AGCM winds at 850 mb are found to be in much better agreement with the observations.

An empirical scheme is developed to reconstruct the AGCM surface wind stress, based on the AGCM winds from 850 mb. The reconstructed wind stress is more consistent with observations for both annual and interannual variability. A series of numerical experiments are conducted using the observed, AGCM, and reconstructed surface stress to force an ocean general circulation model. The results demonstrate that the low-frequency ENSO signals are significantly improved in the OGCM when the reconstructed dataset replaces the original AGCM stress. Improvements are evident in more realistic SST anomalies and variability of the thermocline depth.

1. Introduction

It is well known that the inability of atmospheric general circulation models (AGCM) to produce realistic variability of the surface wind stress over the tropical Pacific is one of the stumbling blocks preventing coupled ocean–atmosphere general circulation models (CGCM) from making successful simulations and predictions of short-term climate variations. Several studies have pointed out specific problems in the quality of AGCM simulated surface wind or wind stress over the tropical Pacific region. Graham et. al (1989a) showed insufficient surface convergence over the intertropical convergence zone (ITCZ) and the warm pool in the mean annual cycles of several wind–wind stress datasets produced by different AGCMs. Using AGCM wind stress to force an ocean general circulation model (OGCM), Gordon and Corry (1991) demonstrated that the model simulated annual cycle in the tropical Pacific Ocean is sensitive to the differences between the observed and AGCM simulated surface stresses and heat fluxes.

Comparing simulations of a linear ocean model forced with observed wind stress anomalies and those simulated by the National Center for Atmosphere Research (NCAR) AGCM, Graham et al. (1989b) showed that the AGCM winds tend to produce weaker and less organized El Niño–Southern Oscillation (ENSO) signals in the tropical Pacific Ocean. Driving an OGCM with wind stress fields simulated by a version of the European Centre for Medium-Range Weather Forecasts (ECMWF) AGCM forced by observed sea surface temperature (SST) during 1970–85, Latif et al. (1990) found that the OGCM-simulated ENSO signals in response to AGCM stress forcing were weak in the eastern Pacific. Ji and Smith (1995) also reported that their OGCM could not reproduce the observed interannual sea level variability in the eastern Pacific when forced with wind stress simulated by the National Meteorological Center (NMC) AGCM with the SST forcing of 1982–93.

Recently, in analyzing surface wind stress simulated by the Center for Ocean–Land–Atmosphere Studies (COLA) AGCM for 1979–91, Huang and Schneider (1995) found that, during boreal spring during the El Niño events of 1983 and 1987, westerly anomalies shifted southward and were replaced by easterly anomalies in the central equatorial Pacific. Using the simulated winds to force an ocean general circulation model, they showed that this kind of wind change generated unrealistic cold anomalies, which propagated along the equator from the western Pacific to the eastern coast in

Corresponding author address: Dr. Bohua Huang, Center for Ocean–Land–Atmosphere Studies, Institute of Global Environment and Society, Inc., 4041 Powder Mill Road, Suite 302, Calverton, MD 20705-3106.
E-mail: huangb@cola.iges.org

about three months, and temporarily eliminated the warm anomalies in the eastern Pacific. They further noted that these wind errors were associated with a systematic southward bias of the AGCM ITCZ, which was most serious during boreal spring, especially during El Niño years.

One potential cause of the errors in AGCM wind stress is the horizontal resolution of the atmospheric model in the Tropics. For example, the narrow convergence zone associated with the ITCZ, and its annual displacement, needs high meridional resolution to be properly represented. The same is true of the sharp SST gradient immediately to the north of the equatorial ''cold tongue,'' the so-called oceanic front. Some sensitivity experiments conducted with the COLA AGCM show a dramatic improvement of the pattern and amount of precipitation associated with the ITCZ when the model horizontal resolution is increased from R15 to R40. However, somewhat surprisingly, there is little improvement of the surface wind stress field near the equator.

In this study we have analyzed model simulated surface wind stress fields, as well as the wind structure within the atmospheric boundary layer. We find that winds are generally better simulated near the top of the boundary layer, for example, 850 mb, than near the sea surface. Using a simple empirical method, we further demonstrate that the surface wind stress fields reconstructed from the winds at a level near the top of the boundary layer are more consistent with the observed surface wind stress than those produced directly by the AGCM. To quantify this improvement we have forced an ocean general circulation model of the Pacific Basin with the original AGCM surface stress, the reconstructed surface stress, and the observed surface stress. We find significant improvement in the OGCM simulated interannual variability when the reconstructed surface wind stress is used to force the model. These results have been used to construct practical schemes that may be useful for correcting systematic errors in coupled GCM simulations and predictions. Prediction experiments using anomaly coupled ocean and atmospheric GCMs with the reconstructed stress fields show large improvements in predictability (Kirtman et al. 1997).

The atmospheric and ocean models used in this study are described in section 2 and observational data in section 3. The AGCM winds are critically examined in section 4, which is followed by a discussion of the OGCM experiments in section 5. The summary and a final discussion is given in section 6.

2. Model descriptions

a. AGCM

The spectral COLA AGCM used for this study has triangular truncation at wavenumber 30 (T30), corresponding to a resolution of about 300 km in the Tropics. The vertical structure of the model is represented by 18 σ-levels. The spacing of the levels is such that greater resolution is obtained near the earth's surface and at the tropopause. The model includes the dynamical effects of mean orography (Fennessy et al. 1994). The physical parameterizations of the COLA AGCM include solar radiative heating (Lacis and Hansen 1974), terrestrial radiative heating (Harshvardhan et al. 1987), deep convection (Kuo 1965, modified), shallow convection (Tiedke 1984), and large-scale condensation. The land surface treatment is based on the Simple Biosphere Model (SiB) biophysical formulation (Sellers et al. 1986) with the Xue et al. (1991) simplification. A general description of the method for prescribing the model boundary conditions can be found in Kinter et al. (1988).

Turbulent transports for heat, momentum, and moisture within the atmosphere are an important physical process within the planetary boundary layer (PBL) and are parameterized based on the Mellor and Yamada (1982) level 2.0 turbulence closure formulation. The depth of the model PBL fluctuates in space and time. The surface layer, where the vertical momentum and heat fluxes are determined by the mixing length theory of Monin and Obukhov (1954), is however prescribed to be 10 mb deep. The surface wind stress is calculated from winds at the lowest level using bulk formulas and a drag coefficient that depends on the surface roughness and the surface layer stability as measured by the Monin–Obukhov length (Long 1988).

The model data used in our analysis are derived from a 10-yr simulation from 1 November 1983 to 31 December 1993 forced with observed monthly SST in the world oceans (Reynolds 1988). The period we have analyzed is from January 1986 to December 1992 when operational analyses of high quality winds are available. We have examined monthly mean surface wind stress and winds below 700 mb.

b. OGCM

The Geophysical Fluid Dynamics Laboratory modular ocean model (GFDL MOM; Pacanowski et al. 1993) is used as a diagnostic tool to evaluate the quality of the datasets of the surface wind stress. This model is a finite difference treatment of the primitive equations of motion using the Boussinesq and hydrostatic approximations in spherical coordinates. The domain is that of the Pacific basin within 30°S–45°N and 130°E–80°W. The coastline and bottom topography are realistic and the maximum depth is set to 4000 m. The zonal resolution was chosen to be 1.5°. The meridional grid spacing is 0.5° between 10°N and 10°S, gradually increasing to 1.5° at 20°N and 20°S. There are 20 levels in the vertical with a constant level interval of 15 m for the top 10 levels. The intervals for the bottom 10 levels are 15.2, 16.1, 20.0, 34.1, 75.9, 177.1, 375.9, 687.4, 1063.8, and 1384.5 m. Richardson number–dependent coefficients are chosen for the vertical mixing and diffusion (Pacanowski and Philander 1981). The horizontal

viscosity and diffusivity coefficients are prescribed as a constant 2×10^7 cm^2 s^{-1}.

The ocean is forced by surface wind stress and heat flux. In these experiments, different surface wind stress datasets are prescribed as forcing fields at the sea surface. The heat flux is composed of radiative, sensible, and latent components. The radiative fluxes are divided into solar and longwave radiation parts. At each time step of the model integration, the solar radiation is prescribed by a linear interpolation of the climatological monthly means analyzed by Oberhuber (1988) from the Comprehensive Ocean–Atmosphere Data Set (COADS). The solar radiation penetrates into the upper ocean with an *e*-folding depth of 12 m. The other components are parameterized as functions of the model SST and a prescribed mean annual surface air temperature, linearly interpolated from climatological monthly observations (Oort 1983). The formulation for longwave radiation is taken from Rosati and Miyakoda (1988), neglecting the effects of cloudiness. The sensible and latent heat fluxes are parameterized by bulk turbulent transfer formulas with parameters as given by Philander et al. (1987).

In the parameterization, the latent and sensible heat, as well as net longwave radiative fluxes, damp the SST departure from a prescribed annual cycle of the climatological air temperature. Therefore, the effect of the heat flux parameterization to the ocean is somewhat similar to that of ones first proposed by Haney (1971) except that the damping rate of the present parameterization is not constant, which depends on the annually and interannually varying surface wind speed. In reality, the air temperature itself changes interannually. However, in a heat flux formulation based on prescribed surface air temperature and model SST, a prescribed interannual signal of the surface air temperature may induce similar SST signals directly and locally, even without wind change. This may obscure the important effects of wind forcing and ocean dynamics in the generation of the SST anomalies. In reality, given an SST change caused by wind forcing/ocean dynamics, air temperature usually follows the SST change and the sensible and evaporative heat fluxes at the sea surface tend to damp the SST anomaly. This process is represented reasonably well by the present parameterization at least in the equatorial waveguide, where the ocean dynamics dominates. This speculation is supported by the comparable magnitudes between simulated and observed SST anomalies around the equator. However, the damping of SST anomalies may be too strong and cause weak SST anomalies in higher latitudes.

The heat flux parameterization used in this model is consistent with those used by some coupled models for ENSO simulation and prediction, such as the Zebiak and Cane (1987) model (referred to as the ZC model hereafter). In the ZC model, SST anomalies with respect to the prescribed SST climatology are damped on a timescale of a few months. In our case, the observed climatological air temperature and constant relative humidity (0.8) are imposed, which ensures the model will reproduce the seasonal cycle of SST because, as we have discussed above, both the air temperature and relative humidity are determined by SST and not the other way around. Moreover, with the present heat flux parameterization SST anomalies are also damped to zero on a timescale of months. The success of the ZC model in simulating ENSO suggests that it is reasonable to use this parameterization for simulating the major aspects of ENSO.

3. Observational datasets

The observational data to be compared with the AGCM output are provided by the European Centre for Medium-Range Weather Forecasts (ECMWF) operational analyses. These data include monthly mean winds at standard pressure levels of 1000, 850, and 700 mb, and the surface wind stress, both for the 7-yr period from January 1986 to December 1992. The relatively recent data from the ECMWF monthly mean time series were selected because spurious variability may be present in the earlier period due to frequent changes in their forecast–analysis system (Trenberth and Olson 1988). The monthly winds are at a resolution of 5° longitude by 4° latitude, which is compatible to the AGCM resolution.

The monthly mean surface wind stress fields are derived from four times daily global wind analyses at 1000 mb, from 0000 UTC 1 January 1986 to 1800 UTC 31 December 1992, as provided by the ECMWF analysis. Since the main purpose of constructing the stress fields is to force the OGCM, which has a finer resolution, high resolution ECMWF data are used. This wind dataset was originally stored in spectral format with a triangular truncation at wavenumber 106 (T106), which was converted to a corresponding spatial grid of Gaussian latitudes (resolution approximately 1° latitude in the Tropics) with a uniform zonal resolution of 1.125° longitude. Then, four times daily fields of the surface wind stress over the oceans were derived from the 1000-mb winds based on the bulk formulae with a constant density and the drag coefficient formulated by Trenberth et al. (1990). The monthly mean stress is constructed by averaging the four times daily wind stress within each month.

Observational ocean datasets used in this study are climatological monthly salinity and temperature produced by Levitus (1982) and monthly mean SST analyzed by Reynolds (1988). The former dataset is constructed based on monthly objective analyses of station data, expendable bathythermograph (XBT) data, and mechanical bathythermograph data on file at the National Oceanographic Data Center. The original data are global on a $1° \times 1°$ grid on chosen vertical levels with intervals increasing from 10 m at the sea surface to 50 m at the depth of 300 m. It is used as initial conditions for the OGCM simulations. The SST data are based on a combination of satellite observations and in situ mea-

surements and are used to examine the simulated SST interannual variability.

The ECMWF analyses are used to validate the AGCM simulations because both the surface and higher-level quantities are derived from the analyses in a physically consistent manner. However, it should be noticed that the analyzed field itself may carry the systematic errors of the numerical weather prediction model, which are not fully corrected through the data assimilation. In fact, a comparison between the daily surface winds from several analysis systems and the in situ measurements at locations over the tropical Pacific showed substantial differences between the analyses and the measurements (Reynolds et al. 1989). Therefore, the quality of the ECMWF analyses should be checked before being used to validate the model.

Our procedure is to use the ECMWF wind stress and another independent dataset to force the OGCM respectively for the period of 1986–91 and then compare the SST anomalies from both simulations with the observations (Reynolds 1988). The latter stress dataset, produced at the Florida State University (FSU), is based on ship observations only (Goldenberg and O'Brien 1981) and is widely used in ocean modeling. Our results show that the correlation between the observed and simulated SST anomalies forced by the ECMWF stress is at least as high as that with the FSU stress forcing in the equatorial Pacific Ocean.

4. AGCM wind analyses

We have examined the AGCM simulated surface wind stress and winds in the lower troposphere both for the mean annual cycle and for interannual variability. Our examination is mainly based on two variables that are characteristic of the circulation within the atmospheric boundary layer. One is the surface wind stress, representing the momentum transport into the ocean and the atmospheric circulation near the surface. The other is the wind at 850 mb, representative of circulation in the middle and upper part of the atmospheric boundary layer.

Figure 1 shows the mean fields of the surface stress and 850-mb wind from the AGCM simulation and from the ECMWF analyses. The most pronounced features of the surface wind stress, from both the simulation (Fig. 1a) and the observations (Fig. 1b), are the northeast and southeast trade winds that lie north and south of the ITCZ. The mean winds at 850 mb, on the other hand, show very weak meridional components (Figs. 1c,d). This is consistent with results of previous studies showing that the convergence is confined to low levels (e.g., Hastenrath and Lamb 1978). The 850-mb winds are mostly easterly over most of the tropical basin with a jetlike center located in the central equatorial Pacific with maximum wind around 8 m s^{-1}.

Although the AGCM simulation is qualitatively similar to the observations at both levels, a close examination shows important differences. For example, at the surface, the ITCZ is farther south in the AGCM wind stress field (Fig. 1a). Moreover, the AGCM wind stresses are stronger than the observations in the major trade wind regions over the eastern ocean, but weaker in the central and eastern Pacific around the equator (Figs. 1a,b). At the 850-mb level, the major difference is in the western ocean north of 5°N, where the ECMWF winds are stronger.

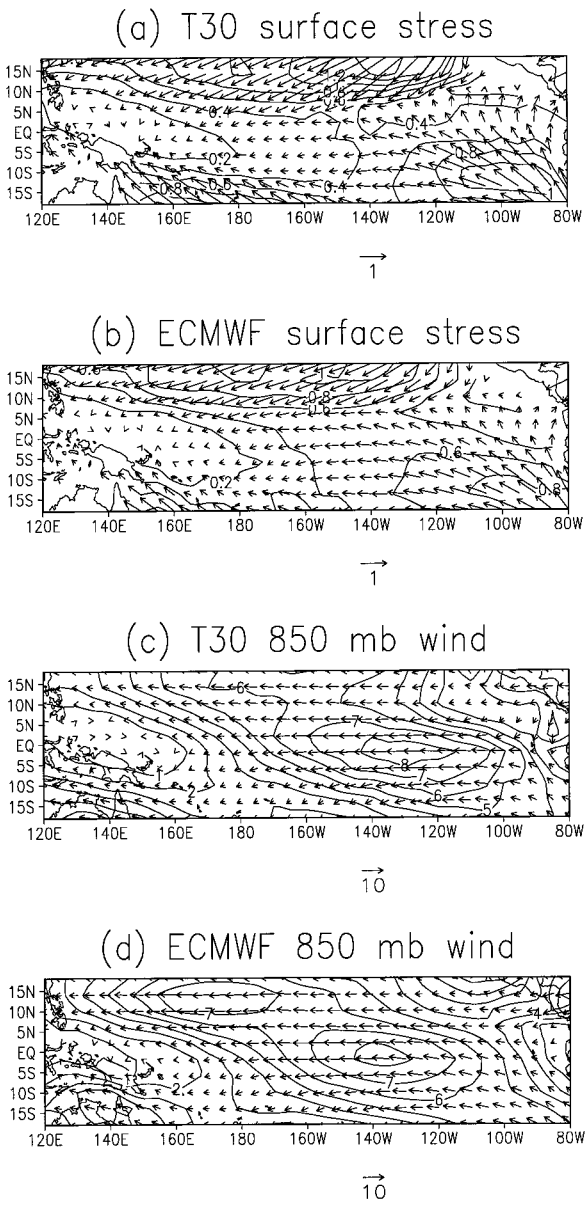

FIG. 1. Mean (1986–92) surface wind stress and wind at 850 mb over the tropical Pacific Ocean. The upper two panels are wind stresses from (a) COLA AGCM simulation and (b) the ECMWF analysis. The lower two panels are 850-mb winds from (c) COLA AGCM simulation and (d) the ECMWF analysis. The units of vectors are represented by the arrows at the right corner of each panel. Superimposed on vectors are the contours of the magnitudes of the wind stress/wind. The contour intervals are 0.2 dyn cm^{-2} for wind stress and 1 m s^{-1} for winds.

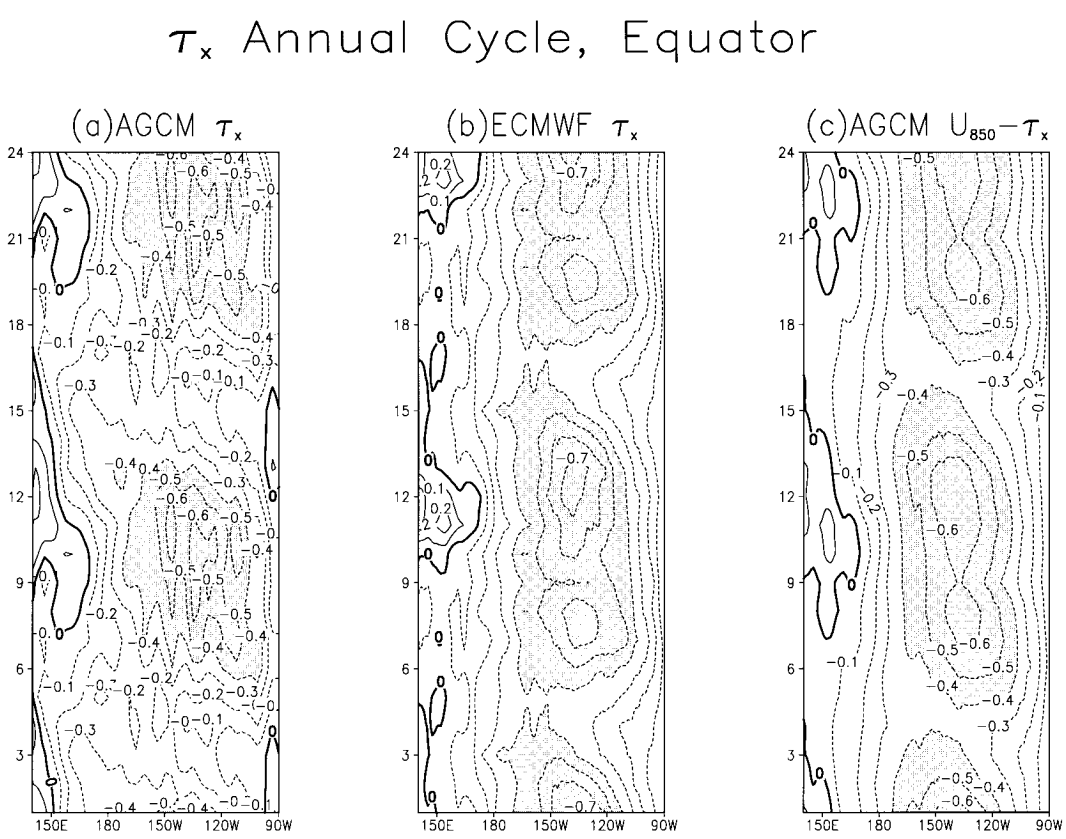

FIG. 2. Mean monthly zonal wind stresses at the equator from (a) AGCM simulation, (b) the ECMWF analysis, and (c) reconstruction ($U_{850} - \tau_x$). Contour interval is 0.1 dyn cm^{-2}. Regions with easterlies larger than 0.4 dyn cm^{-2} are shaded.

In both the AGCM and the observations, the trade wind systems undergo an annual cycle of equatorward migration and zonal expansion into the western Pacific Ocean in the winter and spring of each hemisphere, followed by poleward migration and contraction into the central and eastern ocean during summer and fall. Associated with the fluctuation of the trades, the ITCZ also migrates meridionally. Figures 2a,b depict the annual cycles of the wind stress along the equator for the AGCM and the ECMWF data. For clarity, two annual cycles are shown. In general, they show that easterlies are weakest in boreal spring and persistently stronger in autumn.

There are significant differences between the annual cycles of the surface wind stress from the simulation (Fig. 2a) and the observations (Fig. 2b). Apparently, the model wind stress is too weak throughout the basin from late boreal winter to spring. Moreover, unlike the observed wind stress, which shows two peaks, one in July and the other in December, the AGCM exhibits a single maximum in September. The former problem has been noted by Huang and Schneider (1995), who suggested it may be linked to the fact that the model ITCZ is too close to the equator in boreal spring.

The equatorial winds at 850 mb also undergo a pronounced annual cycle (Figs. 3a,b). According to both the model and observational data, easterly winds are

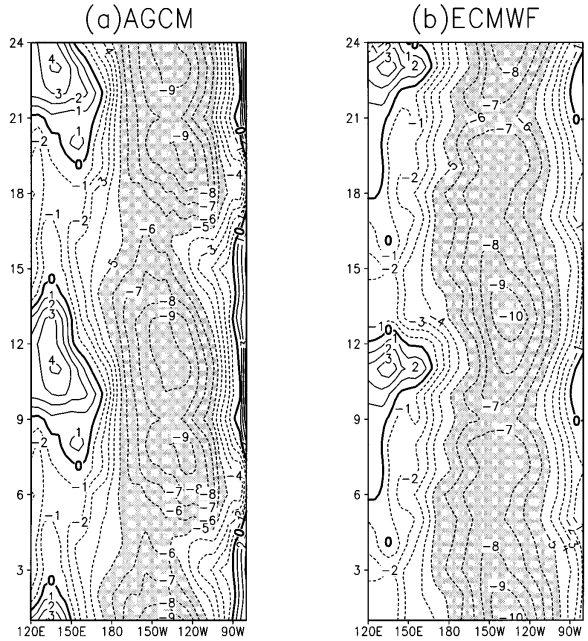

FIG. 3. Mean monthly zonal winds at 850 mb on the equator from (a) AGCM simulation and (b) the ECMWF analysis. Contour interval is 1 m s^{-2}. Regions with easterlies larger than 5 m s^{-1} are shaded.

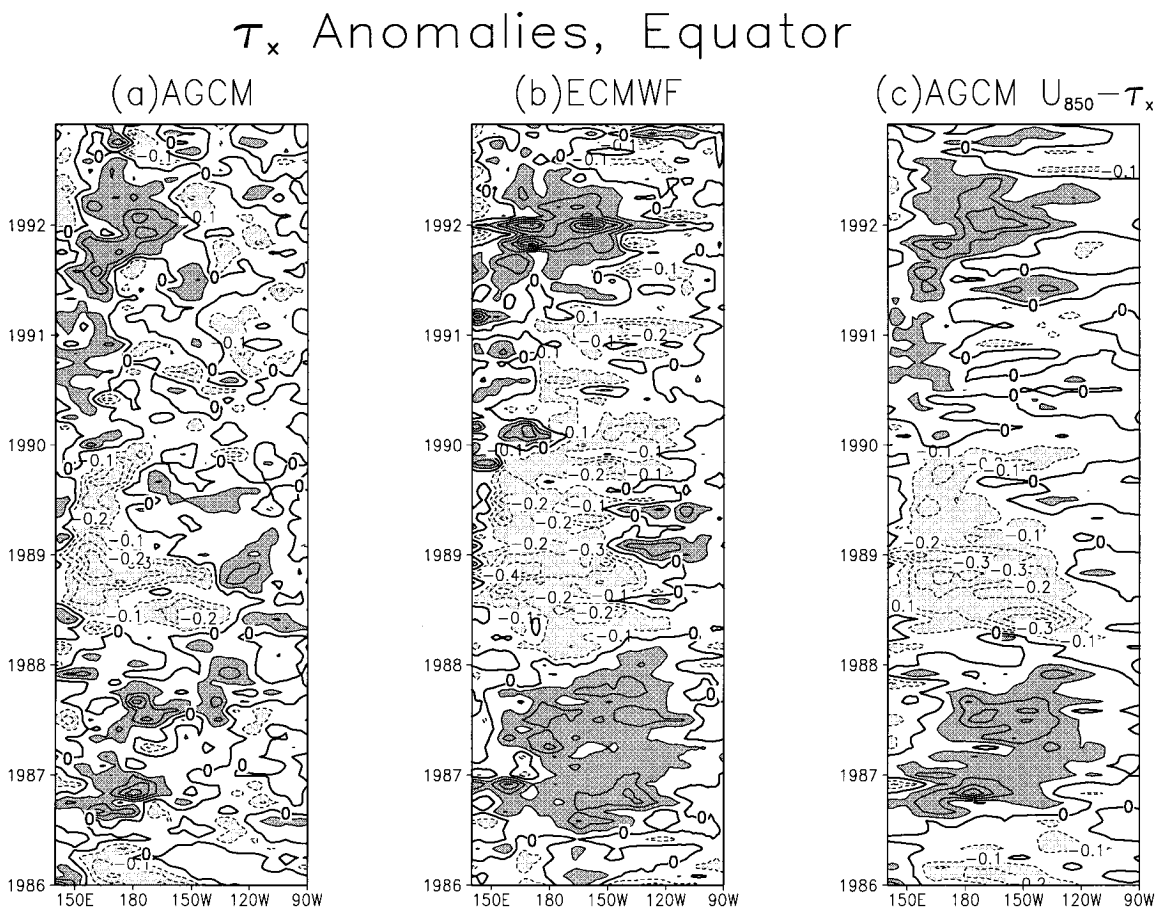

FIG. 4. Monthly anomalies of the zonal wind stresses at the equator from (a) AGCM simulation, (b) the ECMWF analysis, and (c) reconstruction ($U_{850} - \tau_x$). Contour interval is 0.1 dyn cm^{-2}. Regions with anomalies larger than 0.1 dyn cm^{-2} have dark shading and regions with anomalies less than -0.1 dyn cm^{-2} have light shading.

strongest in boreal winter. In the observations, the weakest wind appears in September, just before its rapid intensification (Fig. 3b). Consistent with the observations, the model also presents a wind minimum in September. However, the weakest model winds are in April and May, at the same time when the model surface wind stress is weakest.

Comparing the annual cycles at the surface and at 850 mb, we find two interesting differences between the model and the observations. First, the model surface wind stress is persistently weaker than observed throughout the annual cycle, whereas the AGCM 850-mb winds are generally comparable to or stronger than observed near the equator. We also find that the AGCM 1000-mb winds are weaker than observed. This suggests that the model's momentum mixing within the equatorial boundary layer is inadequate. In fact, the pattern of the AGCM 850-mb wind annual cycle around the equator (Fig. 3b) is more akin to that of the observed surface wind stress (Fig. 2b). In particular, the minimum in boreal spring and the double maxima in July and December are reproduced. This may suggest that the model boundary layer is "deeper" than the observed one. In general, the annual cycle is better simulated at the 850 mb than at the surface.

We have also examined the interannual fluctuations in the zonal stress along the equator (Figs. 4a,b) for the AGCM and the observations, respectively. The major features in the observations (Fig. 4b) are associated with the ENSO cycle, showing alternatively dominant easterly and westerly wind anomalies over the basin with a period of a few years. Associated with a major El Niño event, wind anomalies are in general westerlies from mid-1986 until late 1987, followed by predominantly easterly anomalies during the subsequent La Niña (cold) episode in 1988–89. Strong westerly anomalies then appear in 1991–92, associated with another major warm event.

The major episodes of fluctuations are qualitatively reproduced by the AGCM but with noticeable shortcomings (Fig. 4a). The major signals simulated by the model are confined too much to the west, whereas in the observations they extend eastward in the Pacific basin. Moreover, there are significant higher frequency fluctuations that appear as noise superimposed on the

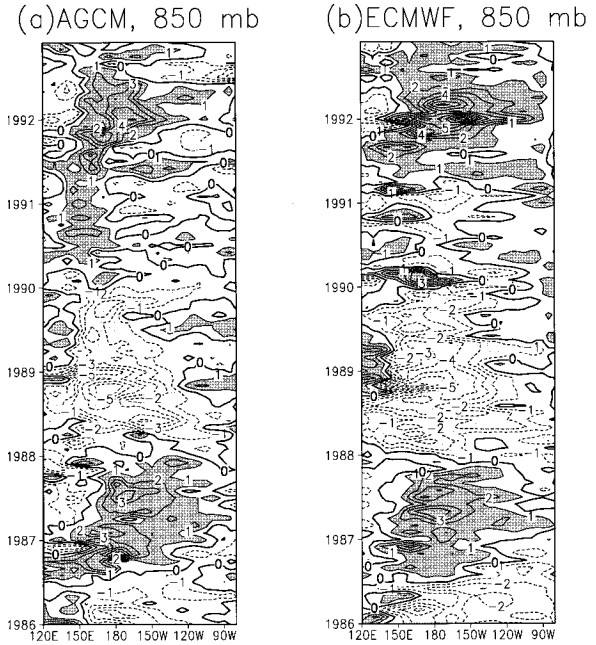

FIG. 5. Monthly anomalies of the zonal winds at 850 mb on the equator from (a) AGCM simulation and (b) the ECMWF analysis. Contour interval is 1 m s^{-1}. Regions with anomalies larger than 1 m s^{-1} have dark shading and regions with anomalies less than -1 m^{-1} have light shading.

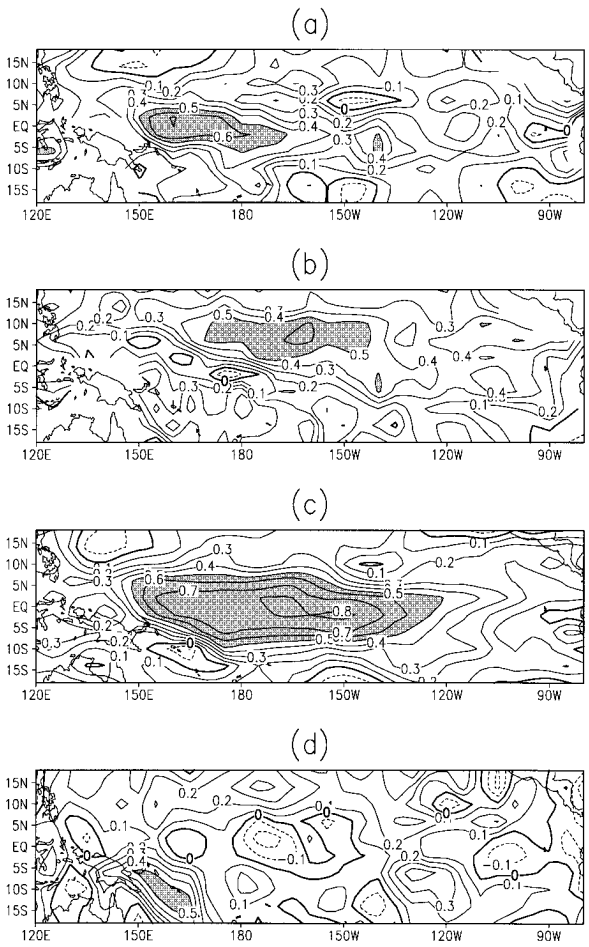

FIG. 6. Correlations between the monthly anomalies of the AGCM and the ECMWF analysis for (a) zonal surface stress, (b) meridional surface stress, (c) zonal winds at 850 mb, and (d) meridional winds at 850 mb. Contour interval is 0.1 with regions of correlations greater than 0.5 shaded.

low-frequency fluctuation. Some of these signals, such as the negative anomaly appearing in the central Pacific during the boreal spring of 1987, are potentially very harmful for ENSO simulation and prediction, as pointed out by Huang and Schneider (1995).

On the other hand, the AGCM simulation and the observations are much more consistent with each other at 850 mb. The interannual fluctuations of the observed zonal wind anomalies (Fig. 5b) are not very different from the anomalies of the observed surface stress (Fig. 4b). Examining the AGCM wind anomaly (Fig. 5a), however, we find that the major errors that seriously degrade the model surface wind stress anomalies are not present at 850 mb. The correlation coefficient between the observations and the simulation (Fig. 6c) is higher than 0.6 over large areas of the equatorial Pacific extending from the western Pacific to about 120°W. The highest correlation (0.8) is over the central Pacific. In comparison, the correlation between model and observed surface stresses is much lower, reaching 0.6 only in the far west. In the eastern Pacific, the model and observed wind stresses are uncorrelated (Fig. 6a).

The correlation analyses further show that, in contradiction to the zonal winds, the model meridional winds are more consistent with the observations at the surface (Figs. 6b,d). The wind fluctuations immediately to the north of the mean ITCZ position are simulated reasonably well by the model over the central Pacific. The observed and model meridional winds have little correlation at 850 mb, which is not surprising because winds at 850 mb are predominantly zonal.

The AGCM has six levels between the surface and 700 mb. We have tried to use the model monthly mean winds at each σ-level to reconstruct the surface wind stress through linear regression of the model wind component to the corresponding component of the observed surface wind stress. We have examined correlations between the observed surface stress and reconstructed surface stress from each of the six layers.

For the four levels below 900 mb, the correlation patterns are very similar to that of the AGCM surface wind stress. A further examination shows that, like the AGCM surface stress, the easterlies at these levels are weakened substantially during boreal spring, followed by a single maximum in September. The major interannual signals are confined to the western ocean. On the other hand, some information on the observed annual and interannual variability of the meridional wind

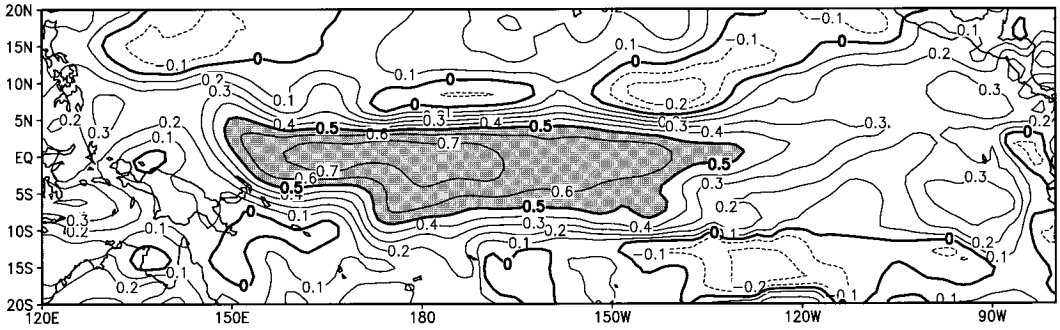

FIG. 7. Correlations between the monthly anomalies of zonal wind stress reconstructed from zonal winds at 850 mb and the ECMWF analysis. Contour interval is 0.1 with regions of correlations greater than 0.5 shaded.

stress appears in the modeled meridional components of the winds at these levels, especially those closer to the surface. The best fit of the meridional component of the observed wind stress is achieved by using the model meridional surface wind stress.

For the two upper levels (approximately 850 and 750 mb), the correlation patterns are similar to the correlations between the observed and the AGCM winds at 850 mb. The zonal component of the observed surface wind stress can be reproduced well, both seasonally and interannually. The results for the model level near 850 mb are generally the best. On the other hand, little variance of the ECMWF meridional wind component can be accounted for by fitting the meridional winds at these levels to the observations. In summary, the best reconstructed surface stress is obtained by using the modeled zonal winds at the AGCM level near 850 mb and the modeled surface meridional wind stress, and we limit further discussion to results from these levels.

The final equation to produce the reconstructed wind stress is given as

$$\tau_x = A_x + B_x U_m \tag{1}$$

$$\tau_y = A_y + B_y V_m, \tag{2}$$

where U_m is the AGCM zonal wind component at the level close to 850 mb and V_m is the AGCM meridional component of the surface stress. The regression coefficients A_x, B_x and A_y, B_y are generated at every grid point by minimizing the root-mean-square differences between the total τ_x, τ_y and their corresponding observations locally. The monthly anomalies of τ_x and τ_y are calculated and multiplied by 1.5 to account for the variance of the observed wind stress anomaly.

This 1.5 amplitude factor is used because we find the magnitude of the reconstructed wind stress anomaly derived from (1) and (2) is weaker than that from the ECMWF analyses. This is possibly because we use the total wind stress for the regression in which the annual cycle is the dominant feature. In fact, the magnitude of the annual cycle is the same between the observations and the model output. The 1.5 factor is multiplied to the anomaly only. This multiplication factor is approximately the ratio between the variances of the observed wind stress anomalies and those derived from the regressions.

The climatological monthly means of τ_x and τ_y and the new anomalies at appropriate months is referred to as the reconstructed dataset of the AGCM wind stress. For simplicity, it will be denoted as $U_{850} - \tau_s$ to reflect the fact that its zonal component is based on winds around the 850-mb pressure level. The 7-yr mean field of this new dataset is the same as the ECMWF analysis from the regression procedure. The reconstructed stress fields are quite smooth compared to the original AGCM stress.

The annual cycle of $U_{850} - \tau_s$ zonal component is shown in Fig. 2c, together with the observations (Fig. 2b) and the original AGCM stress (Fig. 2a). The improvement of the reconstructed wind stress over the original is clear. The easterlies in boreal spring are not as weak, and the double maxima in July and December are clearly shown, although the latter is still a little weaker than observed. The interannual variability is also improved significantly, as shown in Fig. 4c. The correlation between the reconstructed AGCM and observed wind stress anomalies (Fig. 7) is increased significantly in comparison with the original AGCM stress (Fig. 6a). In Fig. 7, large areas in the western and central equatorial Pacific have a correlation of 0.6–0.7. The correlation in the far eastern Pacific is also improved.

We also tried a number of more complicated formulations than (1) and (2), such as combining the two components of the wind vector and using multilevel data to perform the regression. We have also used the pseudowinds as the input for (1) and (2) in order to be more consistent with the bulk aerodynamical formula. However, we did not find further significant improvements. We have therefore adopted the simple formulation given by (1) and (2).

5. OGCM experiments

The reconstructed wind stress data $U_{850} - \tau_s$, the original AGCM wind stress, and the observed surface wind stress are used to force the OGCM for the period 1986–

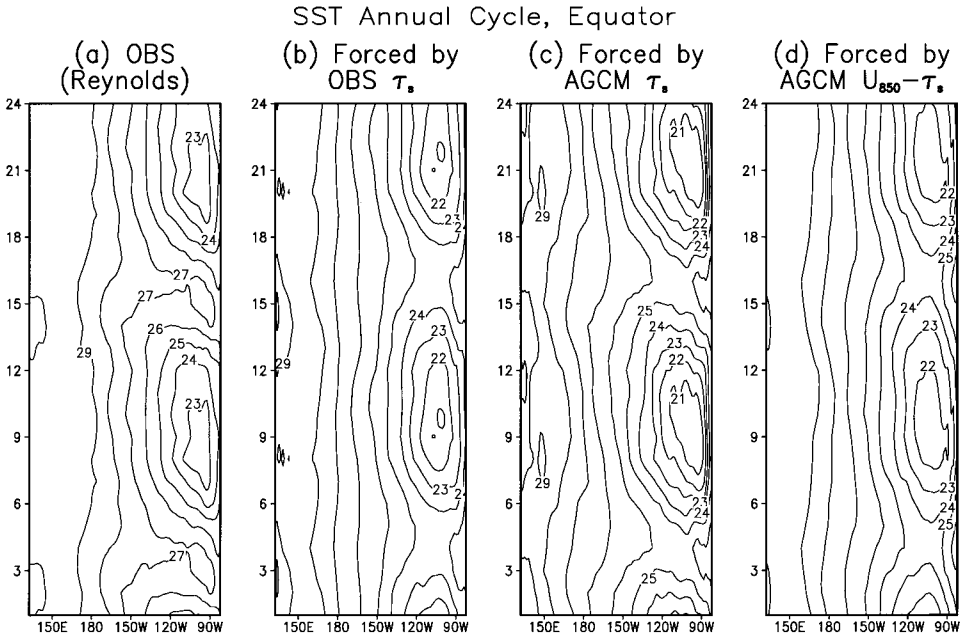

FIG. 8. Time series of equatorial SST mean annual cycle from (a) observations, as well as the OGCM simulations forced by (b) the ECMWF wind stress, (c) the AGCM wind stress, and (d) reconstructed wind stress ($U_{850} - \tau_x$). Two cycles are presented for each panel. The contour interval is 1°C.

92. All the experiments are initialized from an ocean at rest with climatological January temperatures and salinities (Levitus 1982). The model is spun up for three years forced with the monthly climatological wind stress, obtained by averaging the respective datasets during 1986–92.

The climatological monthly mean SSTs along the equator, as derived from the three experiments and the observations, are shown in Fig. 8. The observations (Fig. 8a) show a strong annual cycle in the eastern equatorial Pacific, with SST reaching its maximum in March and its minimum in September. The difference between the maximum and minimum temperatures is about 4°C. The maximum and minimum SSTs coincide with weak southward and strong northward surface wind components, respectively (Horel 1982).

The annual cycle of the equatorial "cold tongue" has been reproduced qualitatively by all the OGCM experiments. However, there is a cold bias in the eastern Pacific in all the simulations (Figs. 8b–d). The SSTs are about 1°–2°C colder than the observations when either the observed or model wind stress is used to force the model. This bias is common for present OGCMs (e.g., Chao and Philander 1993). The amplitude of the annual cycle is strongest when the model is forced with the unmodified AGCM winds (Fig. 8c). The reconstructed stress produces no significant movement in the annual cycle of SST.

The improvement in the interannual variability of SST, however, is remarkable. The equatorial monthly SST anomalies of the period 1986–92 from the observations and the simulations are presented in Fig. 9. The observations (Fig. 9a) clearly show warm and cold episodes over the equatorial ocean associated with the ENSO cycle that are closely related to the zonal wind anomalies on the equator (Figs. 4b, 5b). The SST anomalies derived using the ECMWF stress are quite similar to the observed SST anomalies (Fig. 9b).

In the simulation forced by the original AGCM wind stress (Fig. 9c), SST anomalies are confined to the west. The 1986–87 major warm event, for example, is temporarily disrupted by the reversal of the westerly anomalies in the boreal spring of 1987.

The reconstructed wind stress dataset produces significantly improved SST anomalies (Fig. 9d). In fact, the results are much closer to the simulation using observed wind stress and, in some cases, it is even better. For instance, the distinct warm event in the boreal summer of 1991, which persisted for several months (Fig. 9a) is depicted more clearly in Fig. 9d than in Fig. 9b. Much higher correlations are achieved in the simulations forced with observed and reconstructed wind stresses (Figs. 10a,c) than with the original AGCM stress (Fig. 10b).

Finally, we briefly discuss the interannual variability of the upper-ocean heat content from these simulations. The heat content (HC) is defined as the mean ocean temperature averaged within the upper 232 m, which includes the mixed layer and most of the thermocline. It is an approximate measure of the thermocline depth, sea level, and the dynamic height (Rebert et al. 1985).

Figure 11 presents the HC anomalies along the equator from the three experiments. Heat content anomalies have an eastward phase propagation in these experiments. In the case of the observed forcing (Fig. 11b),

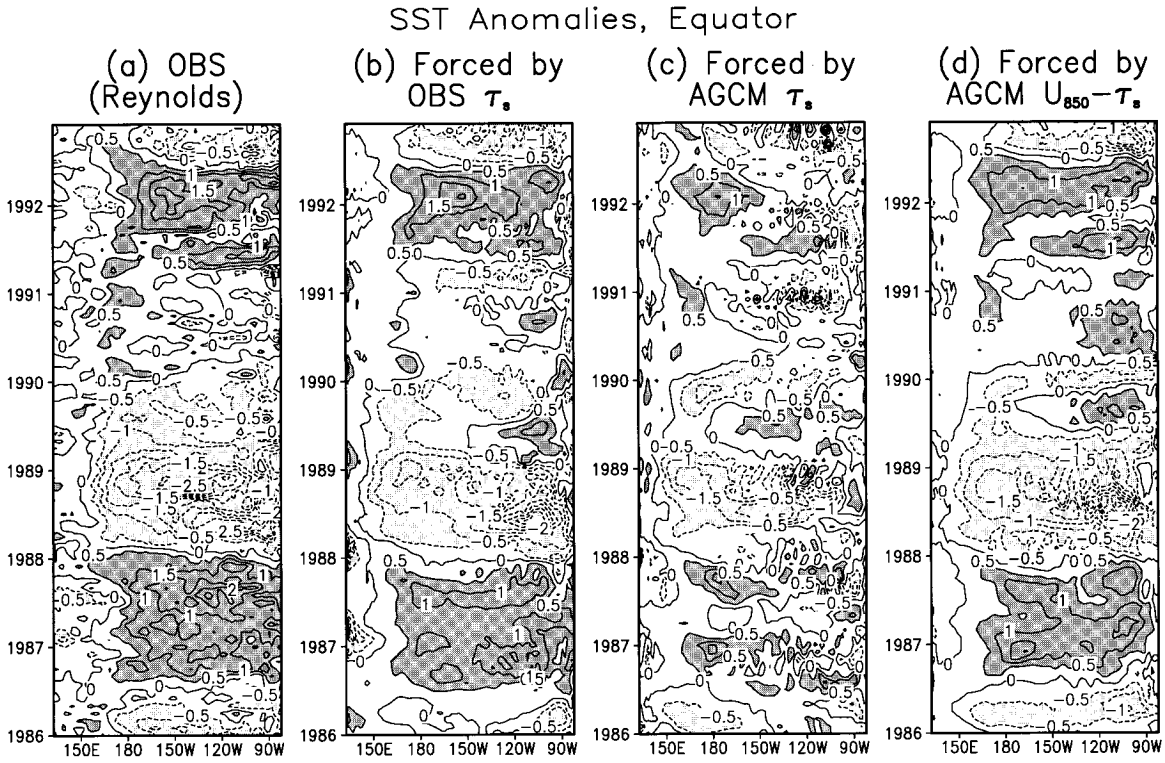

FIG. 9. Time series of equatorial SST anomalies from (a) observations, as well as the OGCM simulations forced by (b) the ECMWF wind stress, (c) the AGCM wind stress, and (d) reconstructed wind stress ($U_{850} - \tau_x$). Contour interval is 0.5°C. Regions with anomalies greater than 0.5°C have dark shading and regions with anomalies less than −0.5°C have light shading.

the 1986–87 and 1991–92 El Niño episodes are associated with positive HC anomalies that propagate eastward and deepen the equatorial thermocline. In the spring of 1986 and 1991, the positive anomalies first appear in the western or central equatorial ocean, then move eastward with intensifying amplitude, first reaching the eastern coast in the boreal summer or autumn. When the anomalous deepening of the thermocline in the eastern ocean is largest negative HC anomalies and shoaling of the equatorial thermocline appear in the western Pacific. These negative HC anomalies then follow a similar eastward progression, reaching the eastern coast in the next summer/autumn.

In the case of the reconstructed wind stress forcing, the low-frequency HC variability is similar to the one described above (Fig. 11c). Signals propagate across the basin smoothly. In the case of the AGCM wind stress forcing, however, the signals are frequently interrupted and rarely propagate to the eastern coast (Fig. 11a). This is also shown by the correlations between the model simulated HC anomalies forced by the ECMWF wind stress and the other two datasets. The correlation between the ECMWF and reconstructed forcing runs (Fig. 12b) is higher than that for the AGCM stress (Fig. 12a) over the equatorial ocean as well as around the eastern coast. This reflects consistent propagation of thermocline disturbances in both the ECMWF and reconstructed forcing cases, first as equatorial waves, then as coastal Kelvin waves after reaching the eastern coast.

6. Summary

We have examined a set of the monthly mean surface wind stress and winds in the lower troposphere for 1986–92, derived from a simulation of an atmospheric general circulation model forced with observed sea surface temperature. It is found that the AGCM surface stress fields have considerable errors. However, the variations of the AGCM winds at 850 mb are more consistent with the observations.

We have developed a simple regression method to reconstruct AGCM surface wind stress based on the zonal winds near 850 mb and the meridional stress at the surface. Through a series of numerical experiments using an ocean general circulation model, we have shown a significantly better simulation of sea surface temperature anomalies and equatorial wave propagation when the reconstructed dataset replaces the original AGCM stress. Our results suggest there are serious deficiencies in the modeling of the planetary boundary layer in the AGCM, especially in the eastern Pacific. The scheme described in this paper to reconstruct the AGCM wind stress can be used as a practical method to correct systematic wind stress errors in coupled

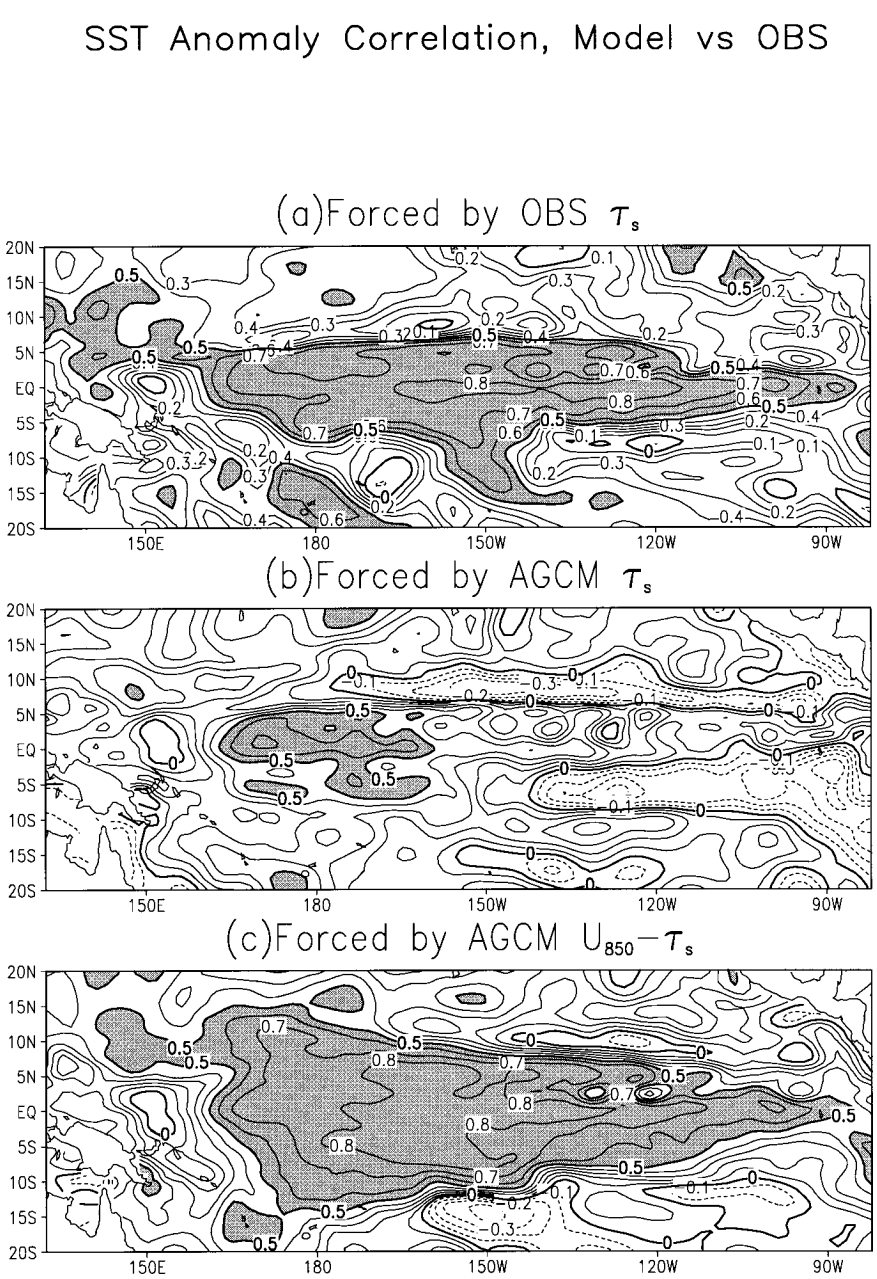

FIG. 10. Correlations between the observed SST monthly anomalies and the OGCM simulated ones forced by (a) the ECMWF wind stress, (b) the AGCM wind stress, and (c) reconstructed wind stress ($U_{850} - \tau_x$). Contour interval is 0.1 with regions of correlations greater than 0.5 shaded.

GCMs. In fact, Kirtman et al. (1997) have shown a dramatic improvement in the skill of ENSO predictions using an anomaly coupled AGCM–OGCM with reconstructed stress fields derived with a scheme similar to the one described here.

There have been several prior efforts in improving AGCM simulated surface stress field through empirical methods. These efforts generally follow the concept of model output statistics (MOS) originally proposed in operational weather forecasting (Glahn and Lowry 1972) to reduce the systematic errors of model output. For example, Latif et al. (1990) have proposed a minimization scheme to the difference between the observed and AGCM simulated surface wind stress. They showed that the minimization can be done either at each model grid point or for the principal components of the leading empirical orthogonal modes. On the other hand, Ji and Leetmaa (1994) and Ji and Smith (1995) corrected the systematic errors of the AGCM stress by using the corresponding modes of the observed and AGCM simulated stress fields derived from a singular-value decomposition (SVD) analysis.

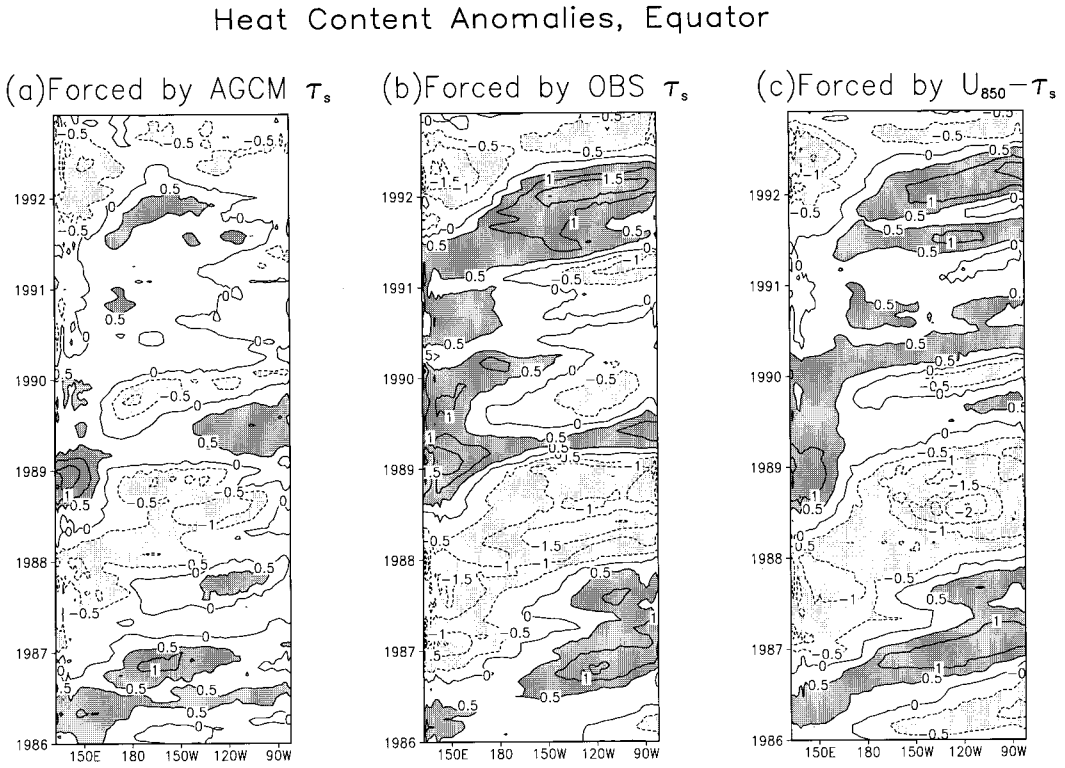

FIG. 11. Time series of equatorial HC anomalies from the OGCM simulations forced by (a) the AGCM wind stress, (b) the ECMWF wind stress, and (c) reconstructed wind stress ($U_{850} - \tau_x$). Contour interval is 0.5°C. Regions with anomalies greater than 0.5°C have dark shading and regions with anomalies less than −0.5°C have light shading.

The method we have used to derive the reconstruction coefficients is similar to the one proposed by Latif et al. (1990). Moreover, through careful analysis, we have chosen the best simulated feature of the lower atmosphere, the zonal wind at 850 mb, for the MOS analysis, instead of using the poorly simulated surface zonal wind stress. We believe that this is important because some of the observed signals are better preserved in the model simulated 850-mb winds.

We recognize that the results do not immediately lead to the conclusion that a coupled GCM using this reconstructed stress will do better than a model coupled with the stress directly produced by the AGCM in long simulations. Simply forcing the ocean with the reconstructed stress in a coupled model will mean that the ocean sees a different stress to the one the atmosphere sees. This inconsistency may cause significant drift of the coupled model mean state in a long-term integration. Some further treatment may be needed to overcome this problem. However, Kirtman et al. (1997) have shown clearly and unambiguously that this procedure improves predictions on seasonal and interannual timescales using an anomaly coupled model.

The empirical correction of the AGCM surface wind stress described here can only be an interim procedure. It is important to understand the origin of these AGCM systematic errors, so that ultimately the treatment of the AGCM boundary layer can be improved such that empirical fixes are not required. Results of this paper, as well as Huang and Schneider (1995), have shown that, in comparison with the ECMWF analyses, the ENSO-related signals are too confined to the western part of the equatorial Pacific. Moreover, in the eastern Pacific unrealistic signals appear in the model wind stress, which interrupt eastward propagating oceanic ENSO signals generated by the wind anomalies in the western and central Pacific Ocean. Similar problems are noticed by Latif et al. (1990) for the ECMWF and by Ji and Smith (1995) for the NMC AGCMs.

It should be noted that surface winds in the Tropics are determined by many factors, such as condensational heating from deep convection (Gill 1980) and SST gradient (Lindzen and Nigam 1987). Gutzler and Wood (1990) pointed out that in the western Pacific the condensational heating plays the major role, whereas the effects of the SST gradient are dominant in the east. At the present time, we suspect that the effects of the SST gradient are not well represented in the COLA AGCM since the errors are mainly in the eastern Pacific. It is also necessary to improve the parameterization of momentum mixing and heat diffusion to simulate the highly baroclinic boundary layer over the eastern part of the tropical Pacific Ocean.

Presently, some of these issues are being investigated

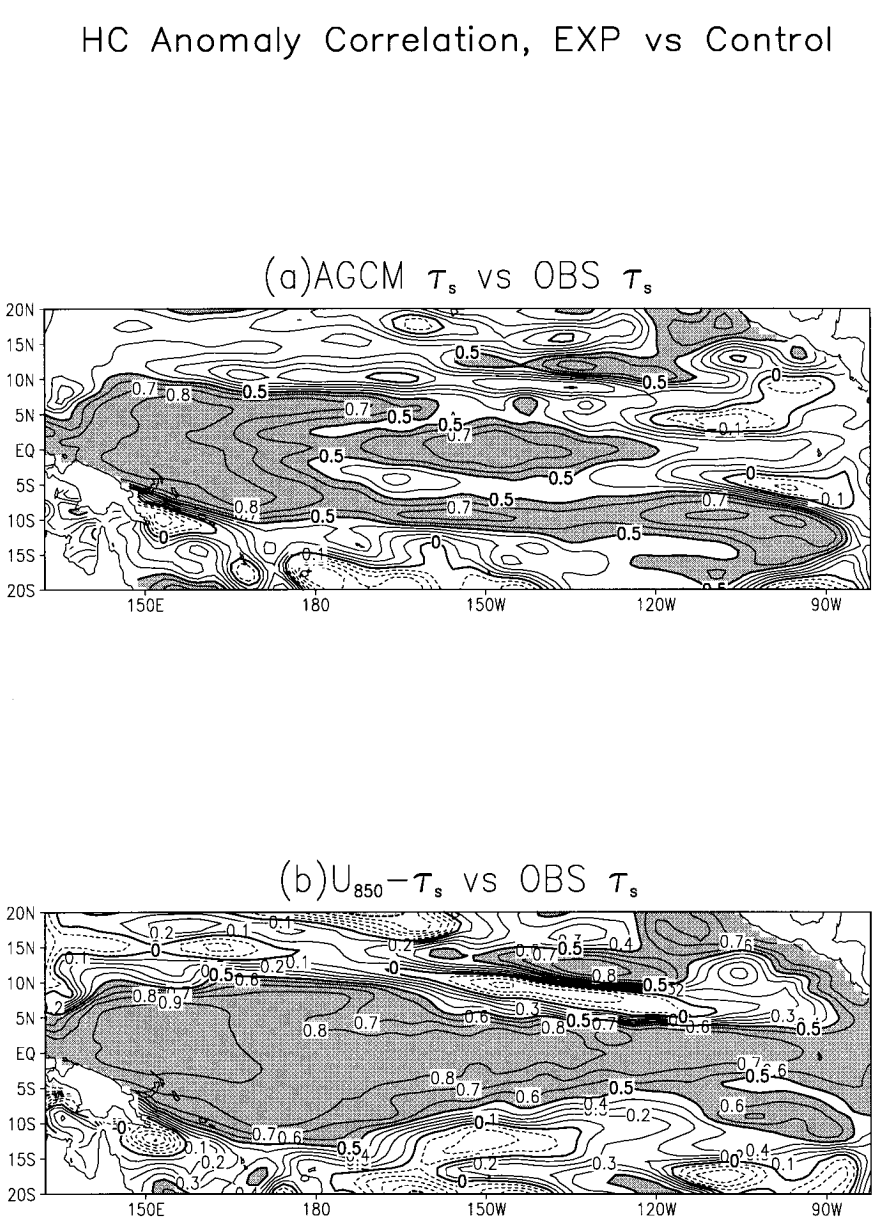

FIG. 12. Correlations between the HC monthly anomalies simulated by the ECMWF forcing and the ones from (a) the AGCM wind stress and (b) reconstructed wind stress ($U_{850} - \tau_x$). Contour interval is 0.1 with regions of correlations greater than 0.5 shaded.

at COLA: a comparison between the surface heat fluxes from the AGCM simulation and the COADS data are conducted. Our preliminary results show that, although there are qualitative similarities between the simulation and the observations in the mean and annual cycle, there are substantial quantitative differences. These differences in surface heat fluxes may be large enough to change the heat balance of the boundary layer significantly. More detailed analysis is in progress. On the other hand, a series of AGCM experiments are being conducted to study the sensitivity of the model simulated wind stress to different parameterizations of the moist convection and turbulent diffusions.

Acknowledgments. The authors are grateful to their colleagues in the Center of Ocean–Land–Atmosphere Studies, especially Drs. E. K. Schneider, J. L. Kinter III, B. Kirtman, Mr. Z. Zhu, Dr. D. DeWitt, Mr. L. Marx, and Mr. M. J. Fennessy, for numerous fruitful discussions regarding this study. We would also like to thank Drs. E. K. Schneider, B. Kirtman, P. Dirmeyer, M. Latif, and two anonymous reviewers for valuable suggestions and comments on the manuscript, and Dr. M. Ji for helpful discussions. Financial support for this research has been provided by the Department of Commence/NOAA under Grants NA26-GP0149 and NA46-GP0217. The OGCM simulations were carried out at

the Florida State University (FSU) CRAY YMP. The AGCM data were provided by Mr. L. Marx. The ECMWF operational analyses were derived from the Data Support Section, Scientific Computing Division, National Center for Atmospheric Research.

REFERENCES

Chao, Y., and S. G. H. Philander, 1993: On the structure of the Southern Oscillation. *J. Climate,* **6,** 450–469.

Fennessy, M. J., and Coauthors, 1994: The simulated Indian monsoon: A GCM sensitivity study. *J. Climate,* **7,** 33–43.

Gill, A. E., 1980: Some simple solutions for heat induced tropical circulation. *Quart. J. Roy. Meteor. Soc.,* **106,** 447–462.

Glahn, H. R., and D. A. Lowry, 1972: The use of model output statistics (MOS) in weather forecasting. *J. Appl. Meteor.,* **11,** 1203–1211.

Goldenberg, S. B., and J. J. O'Brien, 1981: Time and space variability of tropical Pacific wind stress. *Mon. Wea. Rev.,* **109,** 1190–1207.

Gordon, C., and R. A. Corry, 1991: A model simulation of the seasonal cycle in the tropical Pacific Ocean using climatological and modeled surface forcing. *J. Geophys. Res.,* **96**(C1), 847–864.

Graham, N. E., T. P. Barnett, R. M. Chervin, M. E. Schlesinger, and U. Schlese, 1989a: Comparisons of GCM and observed surface wind fields over the tropical Indian and Pacific Oceans. *J. Atmos. Sci.,* **46,** 760–788.

——, ——, V. G. Panchang, O. M. Smedstad, and J. J. O'Brien, 1989b: The response of a linear model of the tropical Pacific to surface winds from the NCAR general circulation model. *J. Phys. Oceanogr.,* **19,** 1222–1242.

Gutzler, D. S., and T. M. Wood, 1990: Structure of large-scale convective anomalies over tropical oceans. *J. Climate,* **3,** 483–496.

Haney, L. R., 1971: Surface boundary condition for ocean general circulation models. *J. Phys. Oceanogr.,* **1,** 241–248.

Harshvardhan, R. Davis, D. A. Randall, and T. G. Corsetti, 1987: A fast radiation parameterization for general circulation models. *J. Geophys. Res.,* **92,** 1009–1016.

Hastenrath, S., and P. Lamb, 1978: On the dynamics and climatology of surface flow over the equatorial oceans. *Tellus,* **30,** 436–448.

Horel, J. D., 1982: On the annual cycle of the tropical Pacific atmosphere and ocean. *Mon. Wea. Rev.,* **110,** 1863–1878.

Huang, B., and E. K. Schneider, 1995. The response of an ocean general circulation model to surface wind stress produced by an atmospheric general circulation model. *Mon. Wea. Rev.,* **123,** 3059–3085.

Ji, M., and A. Leetmaa, 1994: An improved coupled ocean–atmosphere model for ENSO predictions. *Proc. 19th Annual Climate Diagnostics Workshop,* College Park, MD, U.S. Department of Commerce, 88–91.

——, and T. M. Smith, 1995: Ocean model response to temperature data assimilation and varying surface wind stress: Intercomparison and implications for climate forecast. *Mon. Wea. Rev.,* **123,** 1811–1821.

Kinter, J. L., III, J. Shukla, L. Marx, and E. K. Schneider, 1988: A simulation of the winter and summer circulations with the NMC global spectral model. *J. Atmos. Sci.,* **45,** 2486–2522.

Kirtman, B. P., J. Shukla, B. Huang, Z. Zhu, and E. K. Schneider, 1997: Multiseasonal predictions with a coupled tropical ocean–global atmosphere system. *Mon. Wea. Rev.,* **125,** 789–808.

Kuo, H. L., 1965: On formation and intensification of tropical cyclones through latent heat release by cumulus convection. *J. Atmos. Sci.,* **22,** 40–63.

Lacis, A. A., and J. E. Hansen, 1974: A parameterization for the absorption of solar radiation in the earth's atmosphere. *J. Atmos. Sci.,* **31,** 118–133.

Latif, M., J. Biercamp, H. von Storch, M. J. McPhaden, and E. Kirk, 1990: Simulation of ENSO related surface wind anomalies with an Atmospheric GCM forced by observed SST. *J. Climate,* **3,** 509–521.

Levitus, S., 1982: Climatological atlas of the world ocean. NOAA Prof. Paper 13, 183 pp. [Available from NODC, 1825 Connecticut Ave., Washington, DC 20235.]

Lindzen, R. S., and S. Nigam, 1987: On the role of sea surface temperature gradients in forcing low-level winds and convergence in the tropics. *J. Atmos. Sci.,* **44,** 2418–2436.

Long, P. E., 1988: Documentation of the Research Version of the NMC Medium-Range Forecasting Model, National Weather Service/National Oceanic and Atmospheric Administration, chapter 4.

Mellor, G. L., and T. Yamada, 1982: Development of a turbulence closure model for geophysical fluid problems. *Rev. Geophys. Space Phys.,* **20,** 851–875.

Monin, A. S., and A. M. Obukhov, 1954: Basic laws of turbulent mixing in the ground layer of the atmosphere. *Akad. Nauk SSSR Geofiz. Inst. Tr.,* **151,** 163–187.

Oberhuber, J. M., 1988: An atlas based on the ''COADS'' data set: The budgets of heat, buoyancy and turbulent kinetic energy at the surface of the global ocean. Rep. 15, Max-Planck-Institut fur Meteorologie, 199 pp.

Oort, A. H., 1983: Global atmospheric circulation statistics, 1958–1973. NOAA Prof. Paper No. 14, 180 pp.

Pacanowski, R. C., and S. G. H. Philander, 1981: Parameterization of vertical mixing in numerical models of tropical oceans. *J. Phys. Oceanogr.,* **11,** 1443–1451.

——, K. Dixon, and A. Rosati, 1993: The GFDL modular ocean model user's guide, Version 1.0. GFDL Ocean Group Tech. Rep. No. 2., 32 pp. [Available from GFDL/NOAA, Princeton University, Princeton, NJ 08542.]

Philander, S. G. H., W. J. Hurlin, and A. D. Siegel, 1987: Simulation of the seasonal cycle of the tropical Pacific Ocean. *J. Phys. Oceanogr.,* **17,** 1986–2002.

Rebert, J. P., J. R. Donguy, G. Eldin, and E. Wyrtki, 1985: Relations between sea level, thermocline depth, heat content, and dynamic height in the tropical Pacific Ocean. *J. Geophys. Res.,* **90,** 11 719–11 725.

Reynolds, R. W., 1988: A real-time global sea surface temperature analysis. *J. Climate,* **1,** 75–86.

——, K. Arpe, C. Gordon, S. P. Hayers, A. Leetmaa, and M. J. McPhaden, 1989: A comparison of tropical Pacific surface wind analyses. *J. Climate,* **2,** 105–111.

Rosati, A., and K. Miyakoda, 1988: A general circulation model for upper ocean simulation. *J. Phys. Oceanogr.,* **18,** 1601–1626.

Schneider, E. K., and J. L. Kinter III, 1994: An examination of internally generated variability in long climate simulations. *Climate Dyn.,* **10,** 181–204.

Sellers, P. J., Y. Mintz, Y. C. Sud, and A. Dalcher, 1986: A simple biosphere model (SiB) for use within general circulation models. *J. Atmos. Sci.,* **43,** 505–531.

Tiedke, M., 1984: The effect of penetrative cumulus convection on the large-scale flow in a general circulation model. *Beitr. Phys. Atmos.,* **57,** 216–239.

Trenberth, K. E., and J. G. Olson, 1988: An evaluation and intercomparison of global analyses from the National Meteorological Center and the European Centre for Medium-Range Weather Forecasts. *Bull. Amer. Meteor. Soc.,* **69,** 1047–1057.

——, W. G. Large, and J. G. Olson, 1990: The mean annual cycle in global ocean wind stress. *J. Phys. Oceanogr.,* **20,** 1742–1760.

Xue, Y., P. J. Sellers, J. L. Kinter III, and J. Shukla, 1991: A simplified biosphere model for global climate studies. *J. Climate,* **4,** 345–364.

Zebiak, S. E., and M. A. Cane, 1987: A model El Niño–Southern Oscillation. *Mon. Wea Rev.,* **115,** 2262–2278.